Quaternary Research (2024), **117**, 3–18
doi:10.1017/qua.2023.45

Research Article

Late Quaternary glaciations in the Taniantaweng Mountains

Le Chai[a,b,c], Wei Zhang[a], Liang Liu[a], Yapeng Li[a], Qianyu Tang[a], Ruifeng Ma[a], Bo Sun[a] and Jingru Qiao[a]

[a]School of Geography, Liaoning Normal University, Dalian, Liaoning 116029, China; [b]School of Earth Sciences, East China University of Technology, Nanchang, Jiangxi 330013, China and [c]Jiangxi Geological Survey and Exploration Institute, Nanchang, Jiangxi 330009, China

Abstract

Constraining the timing and extent of Quaternary glaciations in the Tibetan Plateau (TP) is significant for the reconstruction of paleoclimatic environment and understanding the interrelationships among climate, tectonics, and glacial systems. We investigated the late Quaternary glacial history of the Qinggulong and Juequ valleys in the Taniantaweng Mountains, southeastern TP, using cosmogenic ^{10}Be surface exposure dating. Four major glacial events were identified based on 26 ^{10}Be ages. The exposure ages of the oldest late Quaternary glaciation correspond to Marine Oxygen Isotope Stage (MIS) 6. The maximum glacial extent was dated to 48.5–41.1 ka (MIS 3), during the last glaciation, and was more advanced than that of the last glacial maximum (LGM). Geochronology and geomorphological evidence indicate that multiple glacial fluctuations occurred in the study area during the Early–Middle Holocene. These glacial fluctuations likely were driven by the North Atlantic climate oscillations, summer solar insolation variability, Asian summer monsoon intensity, and CO_2 concentration.

Keywords: Late Quaternary glaciation, ^{10}Be surface exposure dating, Taniantaweng Mountains, southeastern Tibetan Plateau

INTRODUCTION

Glaciers have shaped the Tibetan Plateau (TP) land surface, as well as its surrounding mountains. The paleoclimatic information preserved in glacial deposits can provide key evidence for exploring the climatic change of the TP since the Quaternary, and the scientific basis for predicting the effects of glacial changes on human environment under future climatic conditions (Immerzeel et al., 2010; Yao et al., 2012).

In recent decades, researchers studied the glacial chronology using in-situ terrestrial cosmogenic nuclide (TCN) exposure dating, which revealed the complex pattern of Quaternary glacial development on the TP (Dortch et al., 2013; Murari et al., 2014). Results show that the Marine Isotope Stage (MIS) 6 represents one of the oldest glacial periods in the semi-arid areas in the central and western TP (Schäfer et al., 2002; Owen et al., 2005), such as the Tanggula Mountains and the more humid southeastern TP (Zhou et al., 2007; Fu et al., 2013; Chevalier and Replumaz, 2019). However, many moraines from this period are poorly preserved, so it remains difficult to explore their actual spatial distribution. After MIS 6, glacial advances of the central and western TP appear to have been most common and widely distributed during MIS 3 (Li et al., 2014; Xu and Glasser, 2015; Blomdin et al., 2016); these glaciers were no smaller than, or may have been even larger than, those of the last glacial maximum (LGM). The glaciers in the humid areas of the southeastern TP reached their greatest extent during the LGM (Owen and Dortch, 2014), although there is a lack of chronological evidence for any glacial development during MIS 3 (Chevalier and Replumaz, 2019). It is thus clear that there are significant regional differences in glacial changes of the TP and its surrounding mountains during the LGM and MIS 3. In addition, recent studies showed that frequent climatic fluctuations during the Holocene triggered multiple glacial advances and retreats in most parts of the TP (Solomina et al., 2015; Saha et al., 2018), although little attention has been paid to the exposure chronology of Holocene glaciers in the southeastern TP.

This article focuses on the central section of the Taniantaweng Mountains, which is located in the western segment of the Hengduan Mountains. This area marks the transitional zone between the southeastern TP and the Yunnan Guizhou Plateau (YGP) (Fig. 1). Using electron spin resonance (ESR) and optically stimulated luminescence (OSL) dating methods, we explored the distribution, evolution, and development of Quaternary glacial landforms on both sides of Yuqu River (Zhang and Chai, 2016; Zhang et al., 2019; Chai et al., 2022). The results constrained at least four glacial stages since the late Quaternary that correspond to MIS 6, MIS 3, MIS 2, and MIS 1. After MIS 6, glaciers gradually decrease. The MIS 6 glaciers were the largest, ranging 25–35 km in length, generally reaching the mouth of glacial valley, and extending down towards the Yuqu River valley. The lengths of glaciers were 12–15 km during MIS 3 and were 7–8 km during MIS 2. Multiple MIS 1 terminal moraines are well preserved within 1–5 km of the termini of modern glaciers. However, ESR dating of glacial deposits is controversial owing to the potential incomplete reset of ESR signals (Yi et al., 2016). In previous studies, a major source of OSL dating uncertainty was whether mineral particles were exposed to sufficient daylight to reset the luminescent signals (Duller, 2006). TCN dating not only can measure the exposure ages of glacial landforms, but also determine the burial ages of moraines, greatly promoting the development of Quaternary glacial chronology in the TP (Heyman et al., 2011; Heyman, 2014; Chen et al., 2015). This study used the TCN dating method to explore the Quaternary glacial sequence of the

Corresponding author: Wei Zhang; Email: zhangweilnu@163.com

Cite this article: Chai L, Zhang W, Liu L, Li Y, Tang Q, Ma R, Sun B, Qiao J (2024). Late Quaternary glaciations in the Taniantaweng Mountains. *Quaternary Research* **117**, 3–18. https://doi.org/10.1017/qua.2023.45

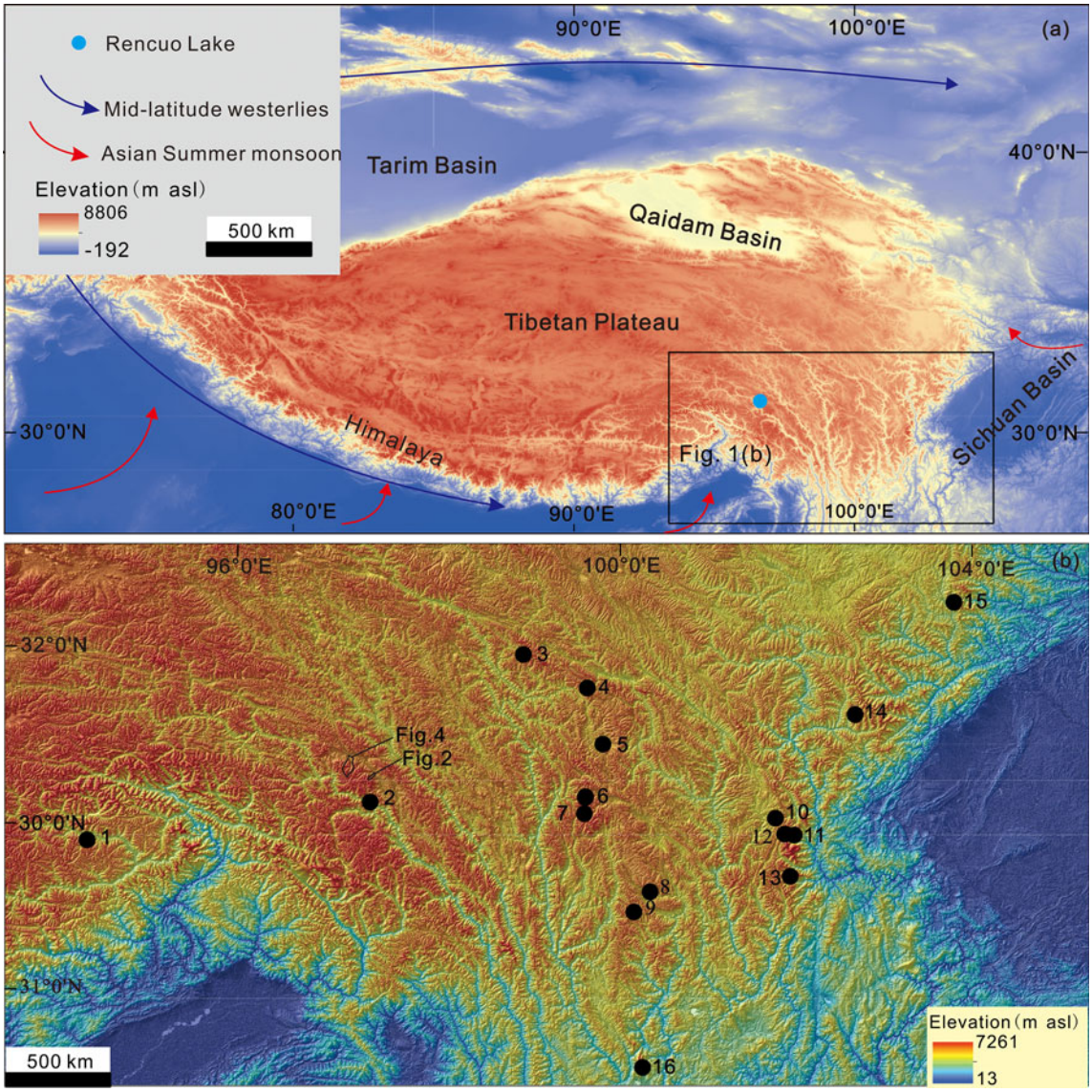

Figure 1. Map showing the study area. (**a**) Shaded relief map of the Tibetan Plateau (TP). (**b**) Relief map of the southeast TP illustrating available ^{10}Be data across the area; locations of Figures 2 and 4 also shown. (1) Basongcuo (Hu et al., 2017); (2) Boduizangbu valley (Zhou et al., 2007); (3) Zhuqin (ZDG) (Chevalier et al., 2018); (4) Ganzi (GZ) (Chevalier et al., 2018); (5) Xinlong Plateau (Graf et al., 2008); (6) Cuopu (Chevalier et al., 2016); (7) Litang County (Schäfer et al., 2002); (8) Gemuxiang (Chevalier and Replumaz, 2019); (9) Daocheng (Fu et al., 2013); (10) Selaha (SLH) (Bai et al., 2018); (11) Yangjiagou (YJG) (Bai et al., 2018); (12) Kandding(KD) (Strasky et al., 2009); (13) Gongga Mountain (Owen et al., 2005; Wang et al., 2023); (14) Siguniang Mountain (Wang et al., 2023); (15) Xuebaoding (Liu et al., 2018); (16) Yulong Mountain (Kong et al., 2009).

study area, which provides important clues for understanding the dynamic processes and mechanisms driving the development of mountain glaciers in monsoonal regions.

REGIONAL SETTING

The central section of the Taniantaweng Mountains (30°40′–30°11′N; 96°39′–97°16′E) is located in the western segment of the Hengduan Mountains. The mountains stretch in a NW-SE direction, with an altitude of ~4000–5500 meters above sea level (m asl). Overall, the Hengduan Mountains are higher in the north than the south, and higher in the west than in the east. The ground surface of this mountain range fluctuates, with an altitudinal difference between its highest and lowest points of <1000 m asl (Su and Pu, 1996). The watersheds of both the Nujiang and Lancang rivers are found in the study area. The main river is the Yuqu River, which is a primary tributary of the Nujiang River. In terms of geological structure, the study area is located within the Changdu Paraplatform, which is bounded by the Nujiang Fault Zone to the west, the Lancang River Fault Zone to the east, and the Wahe–Bangda–Chawalong Fault Zone in its central section. The Yuqu River system developed along a NW-SE fault zone. The exposed strata in the area are mainly composed of granites, limestones, sandstones, and ultrabasic rocks of Devonian, Triassic, and Jurassic periods (Zhang and Chai, 2016).

The area is situated along the South Asian Monsoon (SAM) pathway and has an alpine, continental climate. The advance and retreat of glaciers are closely correlated with fluctuations of the SAM. The mean annual precipitation (MAP) is 474.2 mm, and the mean annual temperature (MAT) is 7.6°C. This area

https://doi.org/10.1017/qua.2023.45 Published online by Cambridge University Press

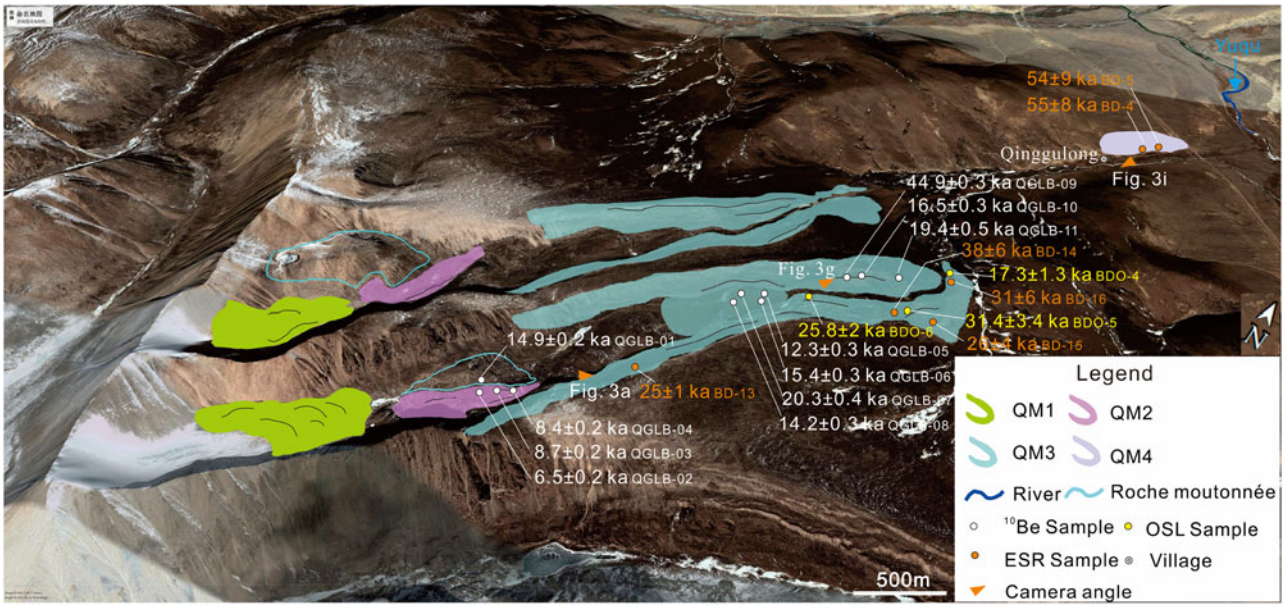

Figure 2. Google Earth image of the study area, showing the locations of moraines in the Qinggulong valley, sampling sites, and ^{10}Be exposure ages.

has clear divisions between dry and wet seasons. Modern glaciers in the study area belong to the transitional zone between marine and subcontinental glaciers and include cirque and hanging glaciers (Su and Pu, 1996). According to the Randolph Glacier Inventory 6.0, which was released in 2017, there are 88 modern glaciers in the study area, covering a total area of 12.955 km^2 (Preffer et al., 2014). The sizes of the glaciers, which are mainly distributed on the western bank of the Yuqu River, are generally small; their termini extend down to 5100–5200 m above sea level (asl). The modern snow line is located at ~5400 m asl.

Quaternary glacial remnants are preserved above 4200 m asl in this area. The distribution of Quaternary glacial erosional and depositional landforms indicates that large-scale piedmont glaciers, valley glaciers, and a large number of cirque glaciers existed in the past.

SAMPLING AND ANALYZING METHODS

Geomorphological mapping and sample collection

Google Earth high-resolution images and a 30-m-resolution digital elevation model (DEM) from the Shuttle Radar Topography Mission (SRTM, http://www.gscloud.cn/sources) were used to identify and map glacial features along the Yuqu River (Zhang et al., 2019), focusing on the Qinggulong and the Juequ valleys (Fig. 1). The morphostratigraphic relationships that we investigated focused on the shape, weathering, and distribution of glacial landforms (Hughes et al., 2005). The relative ages of moraines were established in the field, and compared with other moraine sequences using absolute chronological data from the southeastern TP. The moraines in the Qinggulong and Juequ valleys were named QM4–QM1 and JM5–JM1, respectively. Glacial boulders on the tops of moraine ridges were sampled for ^{10}Be exposure dating. The ideal boulder samples are ones that were not exposed before deposition of moraines, but have been exposed on the tops of moraine ridges since deposition without rolling or surface erosion. This means that the exposure time of boulders closely corresponds to the formation age of the specific moraine ridge (Lal, 1991; Gosse and Phillips, 2001). We used the morphostratigraphic relationships between glacial and associated landforms to determine our sampling strategy. The size and lithology of each boulder were photographed and recorded. The sampling latitude, longitude, and elevation were measured using a handheld global positioning system (GPS) instrument in the field (Zhang et al., 2016). Twenty-six samples were collected from the Qinggulong and Juequ valleys in 2017 and 2018 for ^{10}Be exposure dating, two of which were from bedrock surfaces.

Sample preparation and measurement

All samples were prepared in the Key Laboratory of Tibetan Environment Change and Land Surface Processes, Chinese Academy of Sciences (CAS), Lhasa, followed the methods of Kohl and Nishiizumi (1992). After physical and chemical separation and purification, 20–60 g of pure quartz were dissolved with the addition of ~0.3 mg ^{9}Be carrier. The solution was purified using defluorination and transesterification. Next, ammonium hydroxide was added to the Be solution to prepare hydroxide and dehydrated to extract BeO. Finally, the BeO sample was mixed with Nb powder to create an accelerator mass spectrometry (AMS) measurement target. The ^{10}Be/^{9}Be ratios were measured at the Xi'an Accelerator Mass Spectrometry Centre (Xi'an-AMS Centre), using a certified ratio of 2.851×10^{-12} (Nishiizumi et al., 2007), corresponding to the 07KNSTD standard. The measured isotope ratios were corrected using the values of two blank samples ($4.57 \pm 2.04 \times10^{-15}$ and $1.17 \pm 0.68 \times 10^{-15}$).

Exposure age calculation

All ^{10}Be exposure ages were calculated using the updated CRONUS-Earth V3 calculator (Balco et al., 2008; http://hess.ess.washington.edu/math) and St time-independent (Lal, 1991; Stone, 2000), Lm time-dependent (Balco et. al., 2008), and LSDn production rate (Lifton et al., 2014) scaling. We applied a

https://doi.org/10.1017/qua.2023.45 Published online by Cambridge University Press

default ^{10}Be production rate derived from the primary calibration dataset of Borchers et al. (2016). The ^{10}Be ages and other parameters for the samples are shown in Table 1. The calculation was based on the assumption that the samples collected were not affected by previous exposure or incomplete exposure. The surface erosion rate was assumed to be zero. Because precipitation in the study area may affect the erosion rate of the boulders, we also calculated the dating results under different the erosion rates: 1 mm/ka, 2 mm/ka, and 3 mm/ka. The rock density was set to 2.65 g/cm^3. The topographic shielding factor was calculated using a Python tool and the 30-m ASTER DEM (Li, 2013). Because of dry climatic conditions and sparse vegetation, the snow/vegetation cover at the sampling site was not corrected, potentially underestimating exposure ages. Therefore, each exposure age calculated in this study represents the minimum age. Detailed sample information is provided in Table 1.

This study focused on the calculation of ages based on the LSDn scaling model because the LSDn model predicts scaling behavior more consistently at high-altitude and low-latitude locations (Lifton et al., 2014). To compare with previously published data from the southeastern TP, we recalculated these data using the same scaling model. Both internal and external uncertainties for each ^{10}Be exposure age are reported in Table 2.

Moraine age determination

The age determination of moraines using the TCN dating method is complicated owing geological uncertainties. However, the application of appropriate statistical methods can effectively improve the accuracy of moraine chronologies. We used the Probabilistic Cosmogenic Age Analysis Tool (P-CAAT) (Dortch et al., 2022) to quantitatively exclude outliers in the dataset and to explain the uncertainties in geomorphic processes. The P-CAAT incorporates both sample age and geological uncertainties and uses Monte Carlo simulations to isolate component normal distributions from a cumulative probability density estimate for chronological datasets

Table 1. Cosmogenic^{10}Be surface exposure dating sample details and^{10}Be exposure ages from the Taniantaweng Mountains

Moraine Name	Sample name	Latitude (N°)	Longitude (E°)	Altitude (m asl)	Boulder size L/W/H (m)	Sample thickness (cm)	Topographic shielding factor	Quartz mass (g)	Be carrier (g)	^{10}Be concentration (atom/g)	Error
JM5	JQB-07	30.654	96.907	4569	4.5/2/0.6	2	0.997	30.0158	0.2696	5792000	81700
	JQB-14	30.652	96.904	4531	2/1.6/0.9	1.5	0.997	6.0212	0.3603	820000	50000
	JQB-16	30.652	96.906	4542	3.2/1.6/1.2	3	0.997	23.6138	0.3312	7910000	50000
	JQB-17	30.655	96.905	4506	2.5/1.7/1	1.5	0.997	3.6765	0.3529	2980000	90000
JM4	JQB-05	30.646	96.890	4485	6/3/1.3	1.6	0.997	30.0507	0.255	3269000	596000
	JQB-08	30.647	96.880	4526	2/2.5/1.4	2.9	0.997	4.4309	0.3909	3490000	70000
	JQB-09	30.653	96.881	4489	3/4/7/1/5	2	0.997	8.8701	0.3629	2970000	50000
	JQB-10	30.656	96.884	4462	3.6/4.5/2.6	2	0.997	3.3985	0.3892	5940000	160000
JM3	JQB-02	30.571	96.893	4588	3/1.5/1.3	2	0.983	30.0256	0.264	770400	2940
	JQB-03	30.570	96.893	4596	1.2/0.4/0.6	2	0.982	30.0109	0.2535	1989000	41200
	JQB-22	30.570	96.892	4564	1.3/2/0.9	2	0.982	13.8837	0.3619	1430000	40000
JM2	JQB-24	30.467	96.859	5064	1.5/0.9/0.4	1.5	0.985	19.762	0.3348	520000	20000
	JQB-25	30.468	96.859	5060	1.1/1/0.4	3	0.985	12.763	0.3328	230000	20000
	JQB-27	30.469	96.859	5033	Bedrock	2.5	0.985	7.4144	0.3225	540000	30000
	JQB-28	30.470	96.858	4990	1.3/0.9/0.7	2	0.985	15.3562	0.3139	610000	20000
QM3	QGLB-01	30.429	97.110	5206	Bedrock	2	0.977	51.6117	0.2607	1277000	17600
	QGLB-05	30.443	97.124	5000	3/2/1.6	1.5	0.992	30.0036	0.2704	928000	22300
	QGLB-06	30.443	97.124	5004	1.2/1.1/1	2.6	0.992	30.0211	0.2531	1229000	23700
	QGLB-07	30.442	97.124	5004	2/2.5/1.2	1.5	0.992	28.226	0.2573	1689000	30500
	QGLB-08	30.442	97.124	5005	2/1.5/1.3	1.5	0.994	30.0045	0.2637	1129000	20600
	QGLB-09	30.449	97.133	4884	2.5/1/5	1.2	0.995	30.0202	0.273	3960000	29200
	QGLB-10	30.449	97.133	4863	2.5/1.3/1	2.68	0.994	30.0128	0.2664	1247000	20200
	QGLB-11	30.450	97.134	4846	1/0.7/0.8	1.5	0.995	30.0133	0.2599	1489000	34800
QM2	QGLB-02	30.429	97.110	5201	1.8/1.6/1.5	2.5	0.978	70.6826	0.277	464000	11000
	QGLB-03	30.429	97.112	5193	3/1.8/1.5	3	0.976	41.7965	0.2559	655000	14300
	QGLB-04	30.429	97.112	5198	2.5/1.2/0.7	2	0.976	45.1604	0.2568	635000	12900

[1]Samples JQB-02, 03, 05, 07, QGLG-01–11, with blank of 797133.253 ± 356477.991 at g^{-1} carrier (0.2521 g, 1148.95 ppm Be, $4.57 \pm 2.04 \times 10^{-15}$ ^{10}Be/^{9}Be)
[2]Samples JQB-08–10, 14, 16, 17, 22, 24, 25, 27-28, with blank of 259107.985 ± 149608.950 at g^{-1} carrier (0.3352 g, 1097.1 ppm Be, $1.17 \pm 0.68 \times 10^{-15}$ ^{10}Be/^{9}Be)

https://doi.org/10.1017/qua.2023.45 Published online by Cambridge University Press

Table 2. Apparent ^{10}Be exposure-ages calculated using three scaling schemes.

		St			Lm			LSDn		
Moraine name	Sample name	Age (yr)	Interr (yr)	Exterr (yr)	Age (yr)	Interr (yr)	Exterr (yr)	Age (yr)	Interr (yr)	Exterr (yr)
JM5	JQB-07	89357	1289	7333	81848	1178	6376	80328	1156	4972
	JQB-14	12549	768	1256	13052	798	1266	13090	801	1114
	JQB-16	125372	818	10254	110498	718	8551	107600	699	6560
	JQB-17	46542	1422	3982	41600	1270	3399	40895	1248	2738
JM4	JQB-05	51851	9577	10437	46338	8547	9242	44961	8290	8713
	JQB-08	54735	1113	4523	50074	1017	3937	48539	985	3062
	JQB-09	46964	800	3838	41908	713	3255	41113	699	2549
	JQB-10	96320	2658	8236	87979	2423	7167	86993	2395	5767
JM3	JQB-02	11747	45	932	12401	47	934	12492	48	741
	JQB-03	30386	634	2501	28010	584	2195	27562	575	1735
	JQB-22	21736	611	1832	20925	588	1684	20871	587	1370
JM2	JQB-24	6249	241	550	7078	273	598	7193	277	508
	JQB-25	2801	244	329	3452	300	397	3492	304	367
	JQB-27	6634	369	642	7392	411	691	7475	416	607
	JQB-28	7610	250	652	8463	278	694	8602	283	582
QM3	QGLB-01	14858	206	1196	15058	208	1153	14858	206	904
	QGLB-05	11591	279	960	12306	297	972	12266	296	784
	QGLB-06	15477	300	1263	15570	301	1210	15360	297	957
	QGLB-07	21110	383	1720	20470	372	1587	20251	368	1256
	QGLB-08	14051	257	1143	14344	263	1111	14163	259	878
	QGLB-09	52367	391	4210	47015	351	3585	44853	334	2697
	QGLB-10	16720	272	1354	16684	271	1286	16529	269	1015
	QGLB-11	19923	468	1650	19472	457	1537	19356	455	1234
QM2	QGLB-02	5415	129	447	6342	151	500	6450	153	411
	QGLB-03	7722	169	634	8610	188	674	8721	191	550
	QGLB-04	7408	151	605	8278	169	645	8358	170	523

with three or more samples, using the following formula:

$$t = \sigma + P*\left(\frac{E-I}{A}\right)$$

where t is the total landform-age uncertainty, σ is the one-sigma bound of the Gaussian curve, *P* is the peak of the Gaussian curve, and *E*, *I*, and *A* represent the external uncertainty, internal uncertainty, and ^{10}Be exposure ages, respectively. The cluster degree of the samples was decided by the STD/IQR bandwidth estimator in P-CAAT. The internal uncertainty was used to compare the ^{10}Be exposure ages within the study area, and the external uncertainty was used to compare the exposure ages between different sites.

To ensure an effective comparison with other glacial regions in the southeastern TP, the same P-CCAT method was applied to previously published data, considering only well- and moderately clustered groups with $n \geq 3$ ^{10}Be samples (Dortch et al., 2022). The ^{10}Be ages from some regions failed to meet the above conditions and were excluded (e.g., those of Wang et al., 2006, for which ^{10}Be concentrations and AMS test standards were not available). The chronological results for moraines with two- or single-sample and dispersed boulder-sample groups also were excluded (e.g., Schäfer et al., 2002, Lit 7 sample; Graf et al., 2008, TSO-1 sample; Kong et al., 2009, Renhe valley, Ganheba valley, and Baishui valley; Strasky et al., 2009, K101 sample; Fu et al., 2013, A, F, G, I, K L, O, and R moraines; Zhang et al., 2015, in which there was only one sample per group of moraines; Chevalier et al., 2016, b and f moraines; Liu et al., 2018, M1 moraine in the Yanjin valley, Gr moraine in the Rijiu valley; Chevalier and Replumaz, 2019, inner moraine).

Equilibrium line altitude (ELA) reconstruction

Based on the map of the moraines (Figs. 2, 4), we used the accumulation area ratio (AAR) and area-altitude balance ratio (AABR) methods to calculate the equilibrium-line altitude (ELA) of paleo- and modern glaciers. The AAR method assumes that when the glacier is in a stable state, the ratio of the glacier accumulation area to the total glacier area is fixed. The ratios are typically between 0.50 and 0.80—for middle latitude glaciers, they are between 0.55 and 0.65 (Owen and Benn, 2005), and for mountain

https://doi.org/10.1017/qua.2023.45 Published online by Cambridge University Press

glaciers, they are 0.65 ± 0.05 (Porter, 1975). An AAR value of 0.60 ± 0.05 was used in this study.

The AABR method is based on the principle that the mass balance far from the ELA exceeds that of the nearby mass balance. This method considers both the reconstructed glacier surface height and mass balance gradient. The results show that the average balance ratio (BR) of the 65 glaciers was 1.75 ± 0.71 (Rea, 2009). In this study, we used this ratio to calculate the former ELA. The calculations were performed using the ArcGIS toolbox developed by Pellitero et al. (2015, 2016).

MORAINE SEQUENCE

As illustrated in Figure 2, four sets of moraines are preserved in the Qinggulong valley. The QM4 moraine ridge is preserved at ~4300 m asl on the northeastern side of Qinggulong Village (Figs. 3i, j), and 12 km from the terminal of the glacier. It extends ~50 m, close to Highway 214, 20–25 m above the bed of the Yuqu River. No boulders were found at the top of the moraine ridge, therefore no ^{10}Be samples were collected here.

Moraine QM3 covers an altitudinal range of 4600–5250 m asl and is ~7 km long. The most discernible moraines are the two parallel and symmetrical lateral moraines, and the downstream end moraine ridges (Fig. 3g). The exposed profiles show that the lithology is principally composed of granite and phyllite, with little weathering. Seven boulder samples (QGLB-05, 06, 07, 08, 09, 10, 11) were collected from QM3. A large, polished surface is preserved on the right-hand side of the upper reaches of the QM3 moraine ridge, near the roche moutonnée. The lithology is granite; the top surface (5275 m asl) gently undulates and is 80 m from the cirque floor. Bedrock on the roche moutonnée was sampled (QGLB-01) to date the retreat of the main valley glacier (Fig. 3b).

Terminal moraine QM2 is preserved between 5175 and 5290 m asl downstream from the cirque glacier, 60–75 m above the valley

Figure 3. Main glacial landforms and photographs showing areas sampled in the Qinggulong valley. (**a**) Cirque in the Qinggulong Valley; the pink line represents the QM2 moraine; the green line represents the QM1 moraine; (**b**) view of bedrock sample number QLGB-01; (**c–f, h**) views of boulder samples; (**g**) geomorphology of the Qinggulong Valley; the blue line represents the QM3 moraine; (**i, j**) photographs showing the geomorphic features of moraine QM4.

https://doi.org/10.1017/qua.2023.45 Published online by Cambridge University Press

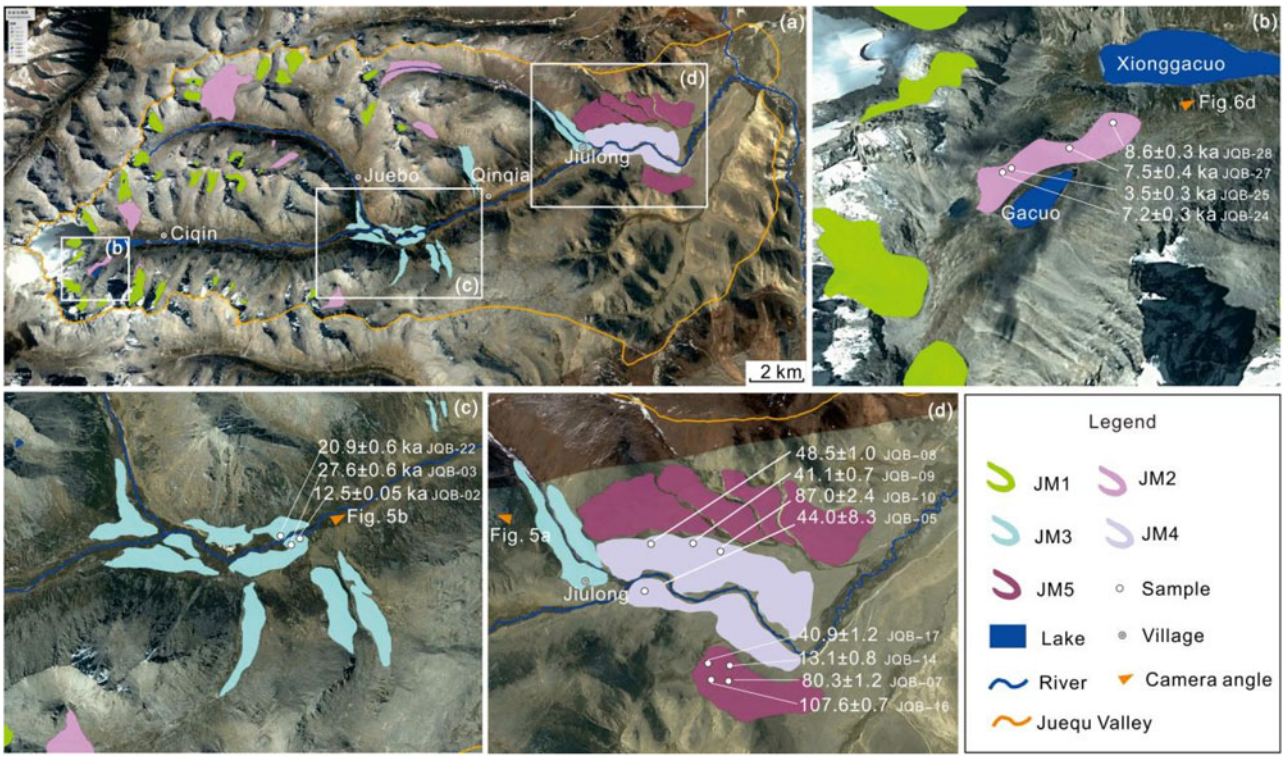

Figure 4. Google Earth images of the study area, showing the locations of moraines in Juequ valley, sampling sites, and ^{10}Be exposure ages.

floor. It is a grayish yellow color and spans the cirque mouth (Fig. 3a, c). Based on an analysis of the exposed section of the moraine ridge, the moraine is mainly composed of granite, with fresh gravels and a low degree of weathering. We collected samples from three QM2 boulders for ^{10}Be exposure dating (QGLB-02, 03, 04).

Terminal moraine QM1 is located at the end of the modern glacier, 80 m above the valley floor (Fig. 3a), at an altitudinal range of 5270–5360 m asl. A large quantity of gravels and small granite boulders are preserved at the top of QM1. No samples were collected from this moraine because there were no suitably large boulders.

The five sets of moraines in the Juequ valley become progressively more weathered and extensive down-valley (Fig. 4). JM5, which is preserved on both sides of the mouth of the Juequ valley (Fig. 5a), indicating the largest glacial extent in this area, is ~25 km from the cirque and 200–300 m higher than the riverbed. Low shrubs (0.5~1 m) grow on top of the moraine, and many granite boulders are scattered on its top. The surfaces of some boulders are extensively weathered. We collected samples from four boulders for ^{10}Be exposure dating (JQB-07, 14, 16, 17).

JM4 is preserved on both sides of the river at the bottom of the Juequ valley mouth (Fig. 5a), reaching 4400–4600 m asl. We collected samples from four of the multiple scattered granite boulders on JM4 for ^{10}Be exposure dating (JQB-05, 08, 09, 10).

JM3 is a terminal moraine (4600–4770 m asl) at the intersection of the main Juequ valley and a branch valley, 13 km from the terminal of the glacier (Fig. 5b). Granite boulders are scattered on the moraine, and low shrubs grow on its top. We collected samples from three boulders for ^{10}Be exposure dating (JQB-02, 03, 22).

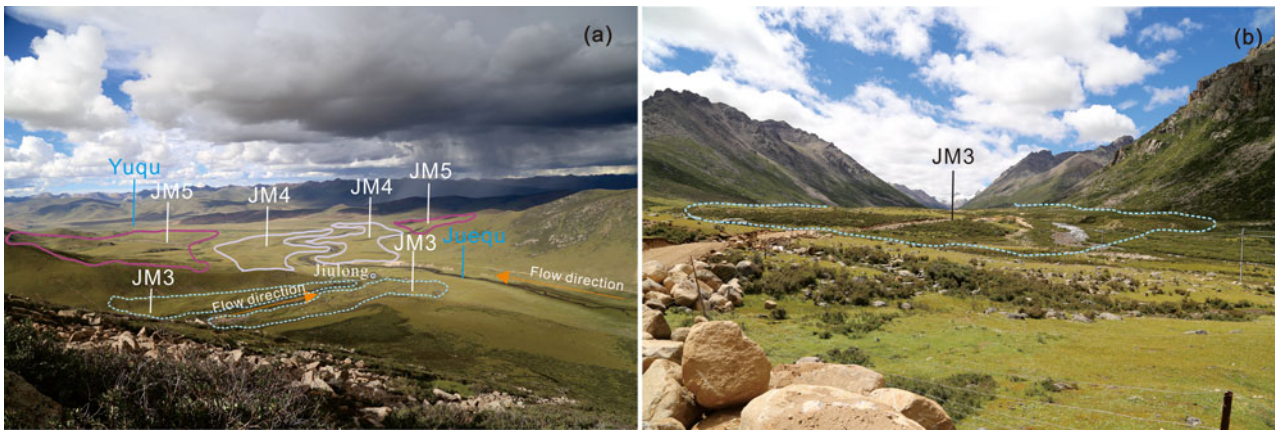

Figure 5. Views of moraines. (**a**) View of the JM5, JM4, and JM3 moraines (tributary valley of the Juequ valley); (**b**) view of the JM3 Moraine (main valley of the Juequ valley).

https://doi.org/10.1017/qua.2023.45 Published online by Cambridge University Press

JM2 moraine (4850–5080 m asl) extends downstream to Xionggacuo, across a roche moutonnée, at the cirque mouth (Fig. 6). We collected samples from three JM2 boulders for ^{10}Be exposure dating (JQB-24, 25, 28), and one sample from bedrock on the roche moutonnée (JQB-27).

JM1 moraine is preserved in the form of an end moraine within 2 km from the terminus of the modern glacier. The granite boulders on top of the moraine were thoroughly intermixed with weathered bedrock, therefore no suitable ^{10}Be samples were found.

RESULTS AND INTERPRETATIONS

The 10 boulder and one polished-surface samples collected from the Qinggulong valley yielded apparent ^{10}Be exposure ages ranging from 44.9 ± 0.3 ka to 6.5 ± 0.2 ka. The 14 glacial boulder and one polished-surface samples from the Juequ valley yielded apparent ^{10}Be exposure ages ranging from 107.6 ± 0.6 ka to 3.4 ± 0.2 ka. The dating results were consistent with the geomorphologic stratigraphy observed in the field. All ^{10}Be ages are shown in Table 2 and Figures 7 and 8.

Qinggulong valley

Seven exposure ages were obtained from Moraine QM3, ranging from 44.9 ± 0.3 ka to 12.3 ± 0.3 ka. The oldest exposure age, 44.9 ± 0.3 ka (QGLB-09), is significantly different from other ages. The sampling location of QGLB-09 was at the front end of the moraine, which might have recycled some boulders exposed prior to the glacial advance. We infer that the QGLB-09 boulder may be related to the glacial event corresponding to the QM4 Moraine, with a much older exposure age. The P-CAAT analysis constrains the age of this moraine to 15.3 ± 2.8 ka (n = 7) (Fig. 7). This age is consistent with previous ages determined using ESR and OSL dating techniques (Fig. 2) (Zhang and Chai, 2016; Zhang et al., 2019), reflecting that a glaciation event occurred in the Qinggulong valley during the late glacial period. The exposure time of a glacially polished surface generally represents the time of glacier disappearance/retreat, if the glacier eroded 2–3 m of bedrock to completely remove the inherited nuclide (Dielforder and Hetzel, 2014). The exposure age of sample QGLB-01 from the ridge of the roche moutonnée suggests that the glacier in the Qinggulong valley retreated or disappeared from this ridge at ca. 14.9 ± 0.2 ka (Fig. 2).

The three samples from QM2 (QGLB-02, 03, 04) yielded ages of 6.5 ± 0.2 ka, 8.7 ± 0.2 ka, and 8.4 ± 0.2 ka, respectively. P-CAAT analysis constrained the age of this moraine to 8.5 ± 0.9 ka (n = 2) (Fig. 7). This indicates that a glacial event occurred during the Early Holocene.

Juequ valley

The four samples from JM5 yielded ages ranging from 107.6 ± 0.6 ka to 14.2 ± 0.9 ka. The P-CAAT analysis showed that the age of this moraine is 96.1 ± 64.0 ka (n = 3) (Fig. 7). Moraine degradation may have led to the overturning or tilting of granite boulders, leading to much younger apparent exposure ages. In addition, field observation indicated that the granite boulders on the surface have undergone obvious weathering and denudation, and some granite boulders have been weathered into detritus. The location, sedimentary profile, and weathered boulders of the moraine all support that this moraine was formed earlier than the oldest sample age obtained. Combining these results with the other chronological and geomorphological characteristics, we infer that this glaciation event may have occurred during MIS 6.

The four samples from JM4 yielded ages ranging from 87.3 ± 2.4 ka to 41.2 ± 0.8 ka. The P-CAAT analysis constrained the age of this moraine to 44.4 ± 10.0 ka (n = 3) (Fig. 7), which suggests that the JM4 moraine recorded a MIS 3 glacial advance. The age 87.3 ± 2.4 (JQB-10) is a potential outlier.

The three samples from JM3 yielded ages ranging from 27.6 ± 0.6 ka to 12.5 ± 0.05 ka. P-CAAT results indicate that the age of 24.8 ± 7.8 ka (n = 2) may represent the time of deglaciation

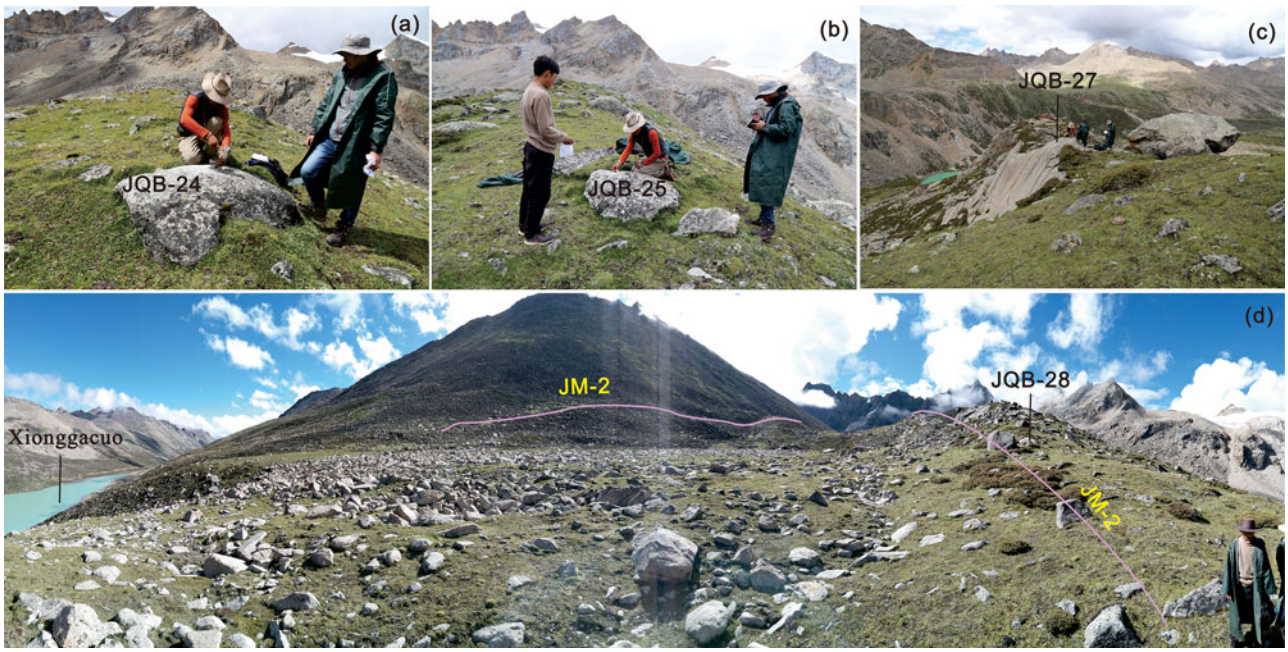

Figure 6. Views of the JM2 moraine and sample localities.

https://doi.org/10.1017/qua.2023.45 Published online by Cambridge University Press

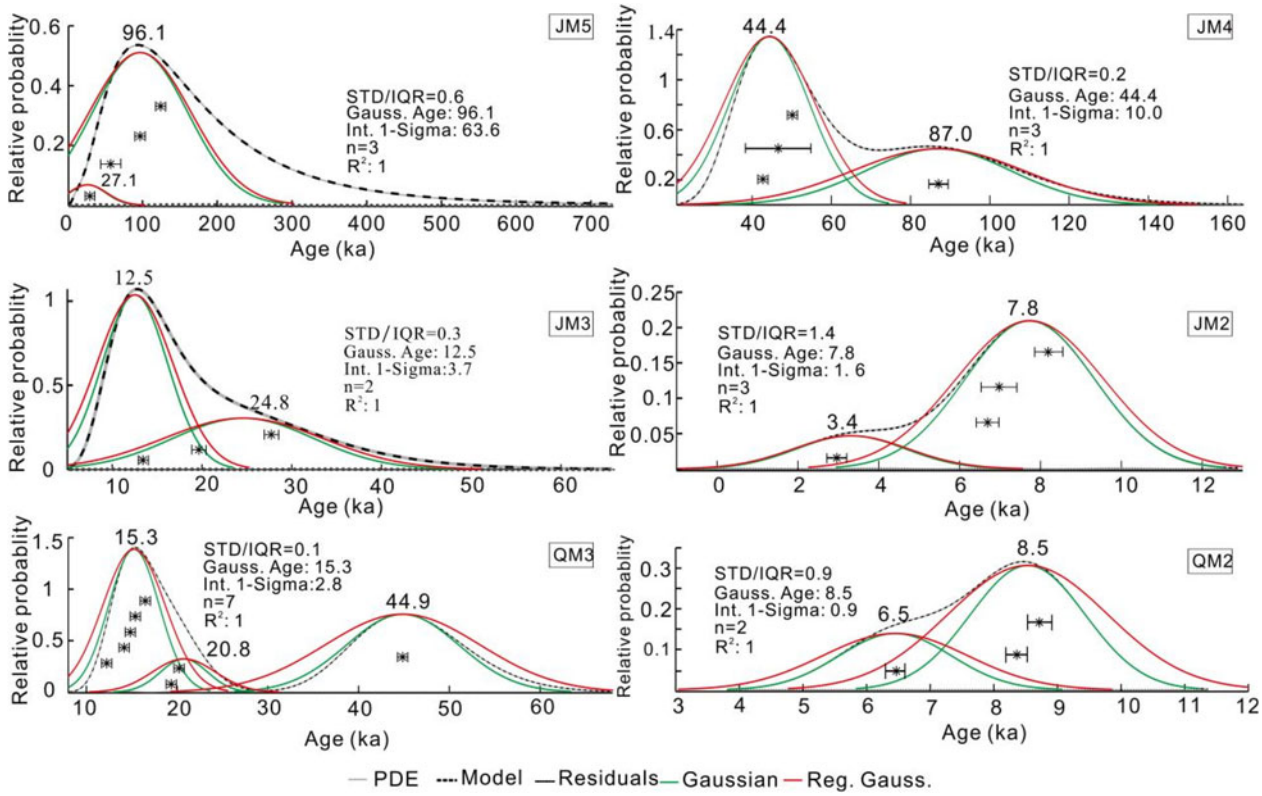

Figure 7. Gauss peak ^{10}Be ages and their uncertainties were analyzed by P-CAAT in two glaciated valleys of the Taniantaweng Mountains. PDE = probability density estimate. The three samples from JM3 yielded ages of 27.6 ± 0.6 ka, 20.9 ± 0.6 ka, and 12.5 ± 0.05 ka. The P-CAAT analysis results indicate that the age of 12.5 ± 3.7 ka (n = 2) may represent the time of deglaciation. However, the most well-preserved TP glacier landform with a true formation age between 8 ka and 44 ka is the moraine ridge during the LGM period (Zhou et al., 2007; Fu et al., 2013; Chevalier et al., 2018). Therefore, JM3 was possibly formed during the LGM, and another peak value of 24.8 ka from P-CAAT analysis may represent the true formation age of JM3.

(Fig. 7), suggesting that the JM3 moraine represents a LGM and transition glaciation event.

The four samples from JM2 yielded ages ranging between 8.7 ± 0.3 ka and 3.4 ± 0.2 ka. The youngest exposure age of 3.4 ± 0.2 ka (JQB-25) is a potential outlier. It was collected from the top of the moraine ridge; the selected boulder may have been affected by a late degradation process, resulting in incomplete exposure. The P-CAAT analysis constrains the age of this moraine to 7.8 ± 1.6 ka (n = 3) (Fig. 7), reflecting an Early Holocene glacial event in the Juequ valley.

In summary, several major glaciation events might have occurred during the late Quaternary in the central Taniantaweng Mountains, corresponding to MIS 6, 3, 2, and 1. Moraine ridges preserved at the termini of modern glaciers (JM1 and QM1) did not yield any usable dates, but investigation of their relative geomorphological characteristics suggests that these moraines may have formed during the Late Holocene. The moraines (JM2 and QM2) are dated to 7.8 ± 1.6 ka and 8.5 ± 0.9 ka, respectively, indicating that a glacial advance occurred during the early Middle Holocene. The dating results for moraines JM3 and QM3 for the last glacial period were 24.8 ± 7.8 ka and 15.3 ± 2.8 ka, respectively, reflecting glacial events during MIS 2. The age extracted from the JM4 moraine ridge (44.4 ± 10.0 ka) indicates a MIS 3 glacial event. Although the application of the ESR dating to Quaternary glacial dating remains controversial, our previous ESR chronology results (54 ± 9 ka and 55 ± 8 ka) for the QM4 moraine in the Qinggulong valley (Zhang and Chai, 2016) were consistent with those of the JM4 moraine in the Juequ valley, indicating that a large-scale glacial advance may have occurred in the central Taniantaweng Mountains during MIS 3. The oldest results for late Quaternary glaciers in the study area may be as old as 96.1 ± 63.6 ka, indicating that there was a large-scale glacial advance in the central Taniantaweng Mountains before the last glacial period that corresponds to MIS 6.

Distribution of ELAs

The paleoglacial ELAs reconstructed using the AAR and AABR methods are listed in Table 3. The ELAs of the modern glaciers in the two glacier valleys were 5392 m and 5530 m. The results showed that the ΔELA value was 614 m during MIS 6. During MIS 3, the ΔELA was 530 m. The ELA for the study area decreased by 368 m and 365 m during MIS 2. During the early Middle Holocene, the ΔELA values were 158 m and 187 m.

DISCUSSION

We summarized 225 previously published ^{10}Be ages of the 40 moraines in southeastern TP to compare and analyze the similarities and differences in the glacial history between the study area and the whole southeastern TP (Fig. 9 and supplementary materials).

Erosion-corrected exposure ages

Table 2 presents minimum exposure ages, assuming an erosion rate of 0 mm/ka in the Taniantaweng Mountains. However, the

https://doi.org/10.1017/qua.2023.45 Published online by Cambridge University Press

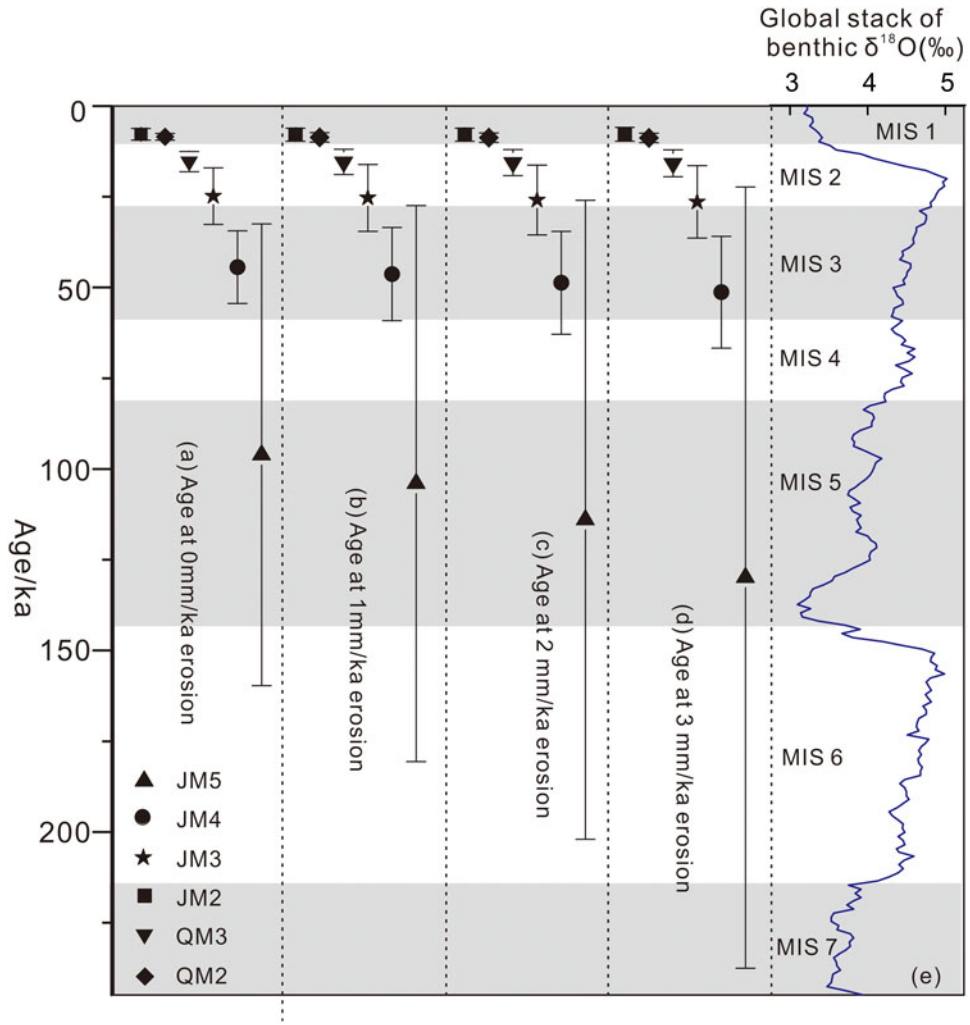

Figure 8. ^{10}Be ages obtained using different rates of erosion for the LSDn production rate model (**a–d**). (**a**) Age with 0 mm/ka erosion rate; (**b**) age with 1 mm/ka erosion rate; (**c**) age with 2 mm/ka erosion rate; and (**d**) age with 3 mm/ka erosion rate. Triangles, circles, stars, and squares represent the ages of boulders on moraines JM5, JM4, JM3, and JM2, respectively. Inverted triangles and diamonds represent the ages of boulders on moraines QM3 and QM2, respectively. (**e**) The blue line is the δ^{18}O record of the global stack (Lisiecki and Raymo, 2005).

erosion rate in the Tibetan Plateau cannot be zero. Wang et al. (2006) estimated the average erosion rate of the bedrock as ~1 mm/ka in the Haizishan area. Therefore, we recalculated the exposure ages of the boulders using erosion rates of 0 mm/ka, 1 mm/ka, 2 mm/ka, and 3 mm/ka for across the southeast TP. The results show that surface weathering and erosion have

Table 3. ELA and ELA depression (ΔELA) for Juequ and Qinggulong valleys (all data are in meters).

		AAR			AABR				
Valley	Period	0.55	0.6	0.65	1.04	1.75	2.46	Mean ELA	ΔELA
Juequ	Contemporary	5434	5434	5384	5384	5384	5334	5392	—
	Early Holocene	5284	5234	5234	5234	5234	5184	5234	158
	MIS 2	5116	5066	5016	5016	4966	4966	5024	368
	MIS 3	4912	4862	4812	4912	4862	4812	4862	530
	MIS 5 or older	4845	4795	4745	4845	4745	4695	4778	614
Qinggulong	Contemporary	5547	5547	5547	5547	5497	5497	5530	—
	Early Holocene	5393	5343	5343	5343	5343	5293	5343	187
	MIS 2	5207	5207	5157	5157	5157	5107	5165	365

https://doi.org/10.1017/qua.2023.45 Published online by Cambridge University Press

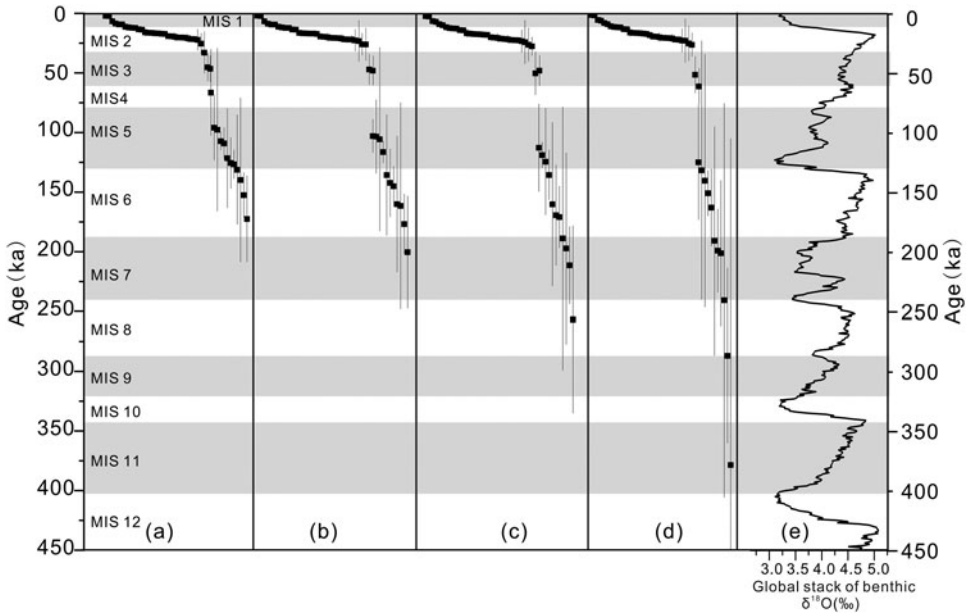

Figure 9. Comparison of ^{10}Be exposure ages with different rates of erosion for the LSDn production rate model in the southeast TP; moraine ages obtained using P-CAAT. (**a**) Age with 0 mm/ka erosion rate; (**b**) age with 1 mm/ka erosion rate; (**c**) age with 2 mm/ka erosion rate; (**d**) age with 3 mm/ka erosion rate; (**e**) δ^{18}O record of the global stack (Lisiecki and Raymo, 2005). See text for details.

significant effects on the exposure age of older samples (e.g., the ages of the JM5 moraine are 96.1 ± 63.6 ka, 104 ± 76.6 ka, 114 ± 88 ka, and 129.9 ± 107.6 ka, respectively) (Fig. 8), but have little effect on the exposure age of relatively young boulders (Fig. 9 and supplementary materials). Thus, the exposure ages discussed below are calculated based on an erosion rate of 1 mm/ka.

Timing of glaciations

MIS 6 glacial stage (102.6–199.6 ka)

The exposure ages of JM5 show that the largest glacial extent occurred in the Taniantaweng Mountains around 104.0 ± 76.6 ka (n = 3). Due to the great uncertainty in surface erosion and snow cover, we suggest that the maximum glacial period in the Taniantaweng Mountains corresponds to MIS 6. Similar ages were found in the Shaluli Mountains (Fu et al., 2013; Chevalier and Replumaz, 2019; Wang et al., 2023). In eastern Nyainqentanglha, the exposure age recorded for the Guxiang glacial period was 160.7 ± 86.6 ka (n = 4, GX-A). Based on the ages of the above moraines, the maximum glacial period in the southeastern TP occurred during MIS 6 (102–199.6 ka).

MIS 3b glacial stage (46.3–47.8 ka)

During MIS 3b (46.3 ± 12.8 ka; n = 3), an important glacial advance occurred in the Juequ valley of the southeastern TP, consistent with the Yulong Mountain results (47.8 ± 11.7 ka, n = 5; Kong et al., 2009). With its abundant precipitation, the MIS 3 glaciation is the most common and extensive glacial stage in High Mountain Asia (HMA) (Chevalier et al., 2011, 2022a; Dong et al., 2014). However, little evidence of a MIS 3b glaciation was found in the 225 exposure ages from the southeastern TP. Xu et al. (2010) obtained three OSL geochronological samples (M2) of 49 ± 4 ka, 58 ± 5 ka, and 45 ± 4 ka from the outer Yingpu valley moraine in the Queer Mountains, indicating that a glacial advance occurred in the region during MIS 3b. Some Chinese scholars have also obtained a small number of chronological results using ESR dating that would appear to indicate a MIS 3b glacial advance on the southeastern TP (Zhao et al., 2007; Wang, 2010).

MIS 2 glacial stage (12.9–25.3 ka)

The recalculated ^{10}Be exposure chronological data show that glacial advances occurred widely between 12.9 ka and 25.3 ka at the southeastern TP (Figs. 1, 9, and supplementary materials), such as eastern Nyainqentanglha, Taniantaweng Mountains, Shaluli Mountains, Daxue Mountains, Siguniang Mountain, and Gongga Mountain. Among the glacial advances at the southeastern TP, most of them were in response to the LGM, while some of them occurred during the late stage of MIS 2.

Younger Dryas (YD) (12.7 ka)

The Younger Dryas event (12.9–11.6 ka) was a global millennium-scale extreme event that occurred during the last glacial–Holocene transition period (Cheng et al., 2020; Gupta et al., 2021). However, in the southeastern TP, only the recalculated ^{10}Be ages of moraines on Xuebaoding Mountain (SCM 2) (Liu et al., 2018) are identified to be corresponding to the YD event. Although researchers think that the differences in scaling models and production rates are one possible reason for the above phenomenon (Wang et al., 2023), the detailed chronology of YD event glaciation in southeastern TP needs to be studied further.

Holocene

In the southeastern TP, glacial advances during the early Middle Holocene and Neoglacial were identified by a small number of ^{10}Be ages and assigned to the Holocene. Exposure age groups JM2 and QM2 show that a glacial event occurred in the Taniantaweng Mountains during the Early Holocene and ended in the early Middle Holocene. In addition to the Taniantaweng Mountains, glacial events from the Early Holocene to Middle Holocene also were identified at Gongga Mountain and Xuebaoding Mountain. This implies that deglaciation occurred in the southeast TP during the Early–Middle Holocene.

https://doi.org/10.1017/qua.2023.45 Published online by Cambridge University Press

Exposure age group CS-A (1.1 ± 0.8 ka, n = 7) shows that a glaciation co-occurred at Gongga Mountain, and RJM1 (1.5 ± 0.2 ka, n = 2) at Xuebaoding Mountain, which is consistent with deglaciation during the Neoglacial. This implies that deglaciation occurred in the southeast TP during the Neoglacial.

^{10}Be, OSL, and ESR age comparisons

The ^{10}Be exposure ages of seven samples collected from the QM3 moraine in the Qinggulong valley ranged between 12.3 ± 0.3 ka and 20.3 ± 0.4 ka (Table 2). The three OSL ages were 17.3 ± 1.3 ka (BDO-4), 31.4 ± 3.4 ka (BDO-5), and 25.8 ± 2 ka (BDO-6) (Zhang et al., 2019). The four ESR ages were 25 ± 1 ka (BD-13), 38 ± 6 ka (BD-14), 26 ± 4 ka (BD-15), and 31 ± 6 ka (BD-16) (Fig. 2). The ESR deposition ages of the QM4 moraine were 54 ± 9 ka (BD-5) and 55 ± 8 ka (BD-4) (Zhang and Chai, 2016). Comparing the results of the ^{10}Be, ESR, and OSL dating methods for the same moraine provides new support for applying cross-dating methods to constrain the ages of glaciation in other areas.

ESR dating measures the number of paramagnetic electrons, which are generated by ionizing radiation (primarily α-, β-, and γ-radiation) of naturally occurring radioactive elements (e.g., U, Th, K) or cosmic ray irradiation trapped in crystal defects. The glacier formation time is determined based on the last zeroing time of the ESR signal, and then used to infer the time of moraine deposition. Accumulated signals produced by paramagnetic Ge-centers in quartz grains have been used commonly for ESR dating of glacial deposits in Central Asia (Yi et al., 2002; Zhou et al., 2002; Zhao et al., 2010). The ESR dating of moraines assumes that moraine sediments experienced glacial grinding or exposure to sunlight, causing their ESR signals to reset. The efficiency of ESR signal resetting has been tested using sunlight bleaching and manual grinding under laboratory conditions. The results showed a 38% loss in the Ge-center ESR signal of crushed quartz after 1 min of manual grinding (Haldorsen, 1981). The study also suggested that the Ge-center signal of quartz for a mixed mineral sample with a thickness >5 mm could not be bleached under natural sunlight within a week, but reached a stable value (Yi et al., 2016). Therefore, the ESR ages of glacial deposits usually constrain the maximum age of glacial termination (Li et al., 2011; Gribenski et al., 2017). In addition, experimental research has shown that the high silt content in moraine sediments results from glacial crushing and abrasion. It can be assumed that moraine sediments have undergone glacial crushing and abrasion, which may reset the quartz Ge-center ESR signal or lead to the signal reaching a stable residual value (Bi et al., 2016). The four ESR samples from QM3 in the Qinggulong valley all had a fine-grained sandy or silty matrix and were collected at depths >50 cm. However, the ages obtained based on the Ge-center signals were significantly older than the TCN ^{10}Be exposure ages, potentially because the Ge-center ESR signals were not completely reset.

The OSL dating technique, which calculates the total amount of ionizing radiation received by detrital minerals, including quartz and feldspar, from radioactive elements, such as U, Th, and ^{40}K, in the surrounding environment since their last burial (i.e., the equivalent dose) and divides it by the amount of ionizing radiation received by the minerals per unit time (i.e., the annual dose) to obtain the burial time of these detrital minerals, has been widely utilized on glacial sediments (Richards, 2000; Owen et al., 2009; Ou et al., 2015). However, the OSL technique has certain limitations in its application on glacial deposits, specifically from inadequate light exposure or incomplete sunlight bleaching (i.e., the luminescence signals were not zeroed before the last deposition, leaving a residual dose in the samples, which may lead to an overestimation of the OSL age) (Duller, 2006; Bateman et al., 2018). Among the three samples for OSL dating, BDO-4 and BDO-6 were taken from the crest of the moraine ridge, where samples were deposited predominantly on the glacier surface, with greater light exposure, thus the luminescence signals of these deposits were more likely to have been zeroed before burial. In addition, the larger-scale glaciation and the long-distance transport of glacial debris also may have increased light exposure. BDO-5 was collected from the middle and lower parts of the moraine ridge, from more complex debris sources. These sediments may not have received adequate light exposure; thus, their dating results are significantly older.

In conclusion, the geomorphic features of the QM3 moraine in the Qingulong valley are clear, showing little influence of post-glacial processes. Compared with the QM4 moraine, the degree of sediment weathering is less. The results of the three dating techniques varied significantly. In general, the ^{10}Be exposure ages were the youngest, followed by the OSL ages, and the ESR ages, which were the oldest. One possible interpretation for this phenomenon is that the results of different dating methods have indicate different processes. The OSL and ESR ages indicate the time of moraine deposition, while the ^{10}Be exposure age indicates the time at which the boulders were exposed on the moraine crests. There may also be a certain time lag between these two events, however, the exact time span is difficult to estimate (Li et al., 2011; Zeng et al., 2019). Another possibility is that the boulders have been susceptible to several other geomorphic processes, such as tumbling, denudation, and burial with sediments, resulting in a younger ^{10}Be exposure age, while the OSL and ESR ages may have been affected by the presence of residual dose in the samples due to incomplete sunlight bleaching.

Possible driving forces of glacial fluctuations

Glacier fluctuations integrate temperature and precipitation signals. Previous studies have shown that North Atlantic climate oscillations (Seong et al., 2009), summer solar insolation variability (Owen et al., 2005), Asian summer monsoon intensity (Owen, 2009), and CO_2 concentration (Schneider et al., 2013) may be the main driving forces of glacier evolution in the TP.

The ^{10}Be results indicate that the southeastern TP experienced multiple glacial fluctuations since MIS 6. The glaciers reached their maximum extent during MIS 6 for the Juequ valley in the Taniantaweng Mountains. Moreover, the morphostratigraphic and geochronological evidence in the Shaluli Mountains shows that the largest range of late Quaternary glaciation in the southeastern TP occurred in MIS 6, and most of the geochronological results are consistent with the periodic variation of summer solar radiation at 60°N in the northern hemisphere (Berger and Loutre, 1991; Dong et al., 2022; Fig. 10), and correspondingly high global ice volumes (Lisiecki and Raymo, 2005; Fig. 10). Research shows that the MIS 6 and MIS 2 glacial periods are the coldest periods in Northern Hemisphere (Lisiecki and Raymo, 2005), with an average temperature of 4–9°C lower than today (Shi, 2002), but the MIS 6 glacial moraine on the TP is more extensive than the MIS 2 glacial moraine, possibly because precipitation during MIS 6 was greater than during MIS 2 (Chevalier et al., 2022b). This is consistent with the conclusion that the Asian monsoon reached its peak during MIS 6 using data from Dongge Cave (Cheng et al., 2016; Fig. 10).

https://doi.org/10.1017/qua.2023.45 Published online by Cambridge University Press

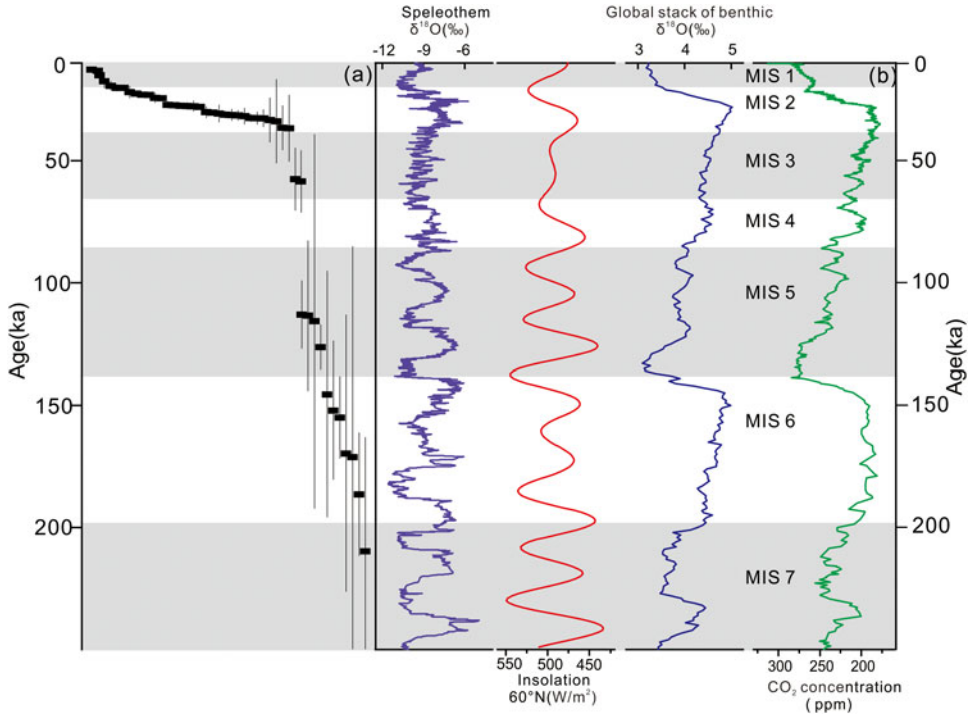

Figure 10. (**a**) All moraine deglaciation ages with 1 mm/ka erosion rate and their uncertainties across the southeast TP; (**b**) selected deglaciation ages from robustly dated moraines in comparison to the speleothem $\delta^{18}O$ records of Dongge Cave (Cheng et al., 2016), the July insolation at 60°N (Berger and Loutre, 1991), the benthic $\delta^{18}O$ record global stack (Lisiecki and Raymo, 2005), and the CO_2 concentration (Bereiter et al., 2015).

Deglaciation ages of the JM4 moraine in the Juequ valley occurred in MIS 3b. The extent of MIS 3b glacier was no less than that during the LGM. Studies have shown that MIS 3b MATs were lower than present by 5°C (Shi, 2002). In Dalijia Shan, Wang et al. (2015) modeling showed that MAP was 50–100% of present, a temperature depression of 4.2–5.6°C, which allowed the formation of abundant snowfall in high-altitude areas (Finkel et al., 2003), producing conditions that were more conducive to glacier development during MIS 3b. A relatively cold and humid climate facilitated glacier development, indicating that a coupled temperature and precipitation control affected glacier activity during this period.

In addition, glaciers advanced across most of the southeastern TP during the LGM. Compared with the conditions necessary for development of MIS 3b glaciers, the intensity of high-latitude summer insolation during the LGM was weaker (Wang et al., 2008; Fig. 10), the effective humidity was reduced (Herzschuh, 2006), global temperatures were 6–9°C lower than present, and MAP was 30–70% less than today (Shi, 2002). A comparative study of pollen data from Rencuo Lake, which is close to Qinggulong, and records of surrounding regions show annual rainfall of only 250 mm in southeastern Tibet, ~40% of the present-day value. The climate in southeastern TP was also cold, with January temperatures 7–10°C and July temperatures 2–5°C lower than present-day values (Tang et al., 2000, 2004). Dry, cold climate conditions may have been the principal factor in development of LGM glaciers on the southeastern TP.

Studies have shown that the development of glaciers on the Tibetan Plateau may have been controlled by the northward movement of the tropical convergence zone and the enhanced monsoonal and increased precipitation during the Early Holocene (Saha et al., 2018, 2019). Pollen data from Rencuo Lake suggest that the SAM became stronger during the Early Holocene, the mean annual temperature was between 0°C and 1°C, and precipitation was higher than present. During the local Early Holocene glacial stage in the Juequ valley, increases in precipitation transported to the area by the SAM were possibly beneficial to the accumulation of glacial ice (Tang et al., 2000; Owen et al., 2005; Thompson et al., 2005; Fig. 10).

Numerous studies have shown that glacial fluctuations during the late Quaternary were related to North Atlantic cooling in the TP, and correlated with the Heinrich Stadials (Hong et al., 2003) and Bond cycles (Wang et al., 2005; Wanner et al., 2011; Dortch et al., 2013; Murari et al., 2014; Solomina et al., 2015). It is noteworthy that the variation trend of atmospheric CO_2 concentration was consistent with glacier advance (Fig. 10) during the late Quaternary in the southeastern TP. Atmospheric CO_2 changes were key components of past climate variability during the last glacial and deglacial periods (Sigman et al., 2010). Antarctic ice core records have shown that changes in CO_2 concentrations on millennium and centennial scales are consistent with abrupt climate changes during the Heinrich and Dansgaard–Oeschger events in the Northern Hemisphere (Bauska et al., 2018, 2021). Researchers have reasoned that CO_2 also may have been a potential factor affecting glacial development (Marcott et al., 2014; Bereiter et al., 2015; Dong et al., 2020). Thus, fluctuation of late Quaternary glaciers in the southeast TP might be the result of several factors, including insolation changes, Asian summer monsoon intensity, North Atlantic cooling event, and/or changes in CO_2 concentration.

CONCLUSIONS

Twenty-six ^{10}Be exposure ages from the Juequ and Qinggulong valleys in the central Taniantaweng Mountains constrained four

https://doi.org/10.1017/qua.2023.45 Published online by Cambridge University Press

glacial events in the late Quaternary, corresponding to MIS 6, MIS 3, MIS 2, and MIS 1. These results supplement the chronological database of late Quaternary glaciations in the southeastern TP. The oldest glaciation in the study was formed at MIS 6. The MIS 3 glacier was much more extensive than that during LGM glacial events in our study area. In addition, both geochronological and geomorphological evidence indicate that glacial fluctuations occurred during the Early to Middle Holocene (8.5–7.7 ka). North Atlantic climate oscillations, summer solar insolation variability, Asian summer monsoon intensity, and CO_2 concentration are possible influence factors for late Quaternary glacier fluctuations in the study area.

Supplementary Material. The supplementary material for this article can be found at https://doi.org/10.1017/qua.2023.45

Acknowledgments. This work was supported by the National Natural Science Foundation of China (Grant Nos. 42071013, 41671005), the Doctoral Scientific Research Foundation of East China University of Technology (Grant No. DHBK2019005), the Opening Foundation of the Key Laboratory of Digital Land and Resources of the East China University of Technology (Grant No. DLLJ202111).

Data availability. All data included in this study are available upon request by contact with the corresponding author.

REFERENCES

Bai, M., Chevalier, M.L., Pan, J., Replumaz, A., Leloup, P.H., Métois, M., Li, H.B., 2018. Southeastward increase of the late Quaternary slip-rate of the Xianshuihe fault, eastern Tibet. Geodynamic and seismic hazard implications. *Earth and Planetary Science Letters* **485**, 19–31.

Balco, G., Stone, J.O., Lifton, N.A., Dunai, T.J., 2008. A complete and easily accessible means of calculating surface exposure ages or erosion rates from ^{10}Be and ^{26}Al measurements. *Quaternary Geochronology* **3**, 174–195.

Bateman, M.D., Swift, D.A., Piotrowsk, J.A., Rhodes, E.J., Damsgaard, A., 2018. Can glacial shearing of sediment reset the signal used for luminescence dating? *Geomorphology* **306**, 90–101.

Bauska, T.K., Brook, E.J., Marcott, S.A., Baggenstos, D., Shackleton, S., Severinghaus, J.P., Petrenko, V.V., 2018. Controls on millennial-scale atmospheric CO_2 variability during the last glacial period. *Geophysical Research Letters* **45**, 7731–7740.

Bauska, T.K., Marcott, S.A., Brook, E.J., 2021. Abrupt changes in the global carbon cycle during the last glacial period. *Nature Geoscience* **14**, 91–96.

Bereiter, B., Eggleston, S., Schmitt, J., Nehrbass-Ahles, C., Stocker, T.F., Fischer, H., Kipfstuhl, S., Chappellaz, J., 2015. Revision of the EPICA Dome C CO_2 record from 800 to 600 kyr before present. *Geophysical Research Letters* **42**, 542–549.

Berger, A., Loutre, M.F., 1991. Insolation values for the climate of the last 10 million years. *Quaternary Science Reviews* **10**, 297–317.

Bi, W.L., Yi, C.L., 2016. Review of ESR dating technique in Quaternary glacial chronology. *Journal of Glaciology and Geocryology* **38**, 1292–1299. [in Chinese, with English Abstract]

Blomdin, R., Stroeven, A.P., Harbor, J.M., Lifton, N.A., Heyman, J., Gribenski, N., Petrakov, D.A., *et al.*, 2016. Evaluating the timing of former glacier expansions in the Tian Shan: a key step towards robust spatial correlations. *Quaternary Science Reviews* **153**, 78–96.

Borchers, B., Marrero, S., Balco, G., Caffee, M., Goehring, B., Lifton, N., Nishiizumi, K., Phillips, F., Schaefer, J., Stone, J., 2016. Geological calibration of spallation production rates in the CRONUS-Earth project. *Quaternary Geochronology* **31**, 188–198.

Chai, L., Zhang, W., Liu, L., Ma, R.F., Tang, Q.Y., Li, Y.P., Qiao, J.R., 2022. Study on early-mid Holocene glacial advance events in the Taniantaweng Mountains, southeastern Qinghai-Tibet Plateau. *Journal of Glaciology and Geocryology* **44**, 307–315. [in Chinese, with English Abstract]

Chen, Y.X., Li, Y.K., Wang, Y.Y., Zhang, M., Cui, Z.J., Yi, C.L., Liu, G.N., 2015. Late Quaternary glacial history of the Karlik Range, easternmost Tian Shan, derived from ^{10}Be surface exposure and optically stimulated luminescence datings. *Quaternary Science Reviews* **115**, 17–27.

Cheng, H., Edwards, R.L., Sinha, A., Spötl, C., Yi, L., Chen, ST., Kelly, M., *et al.*, 2016. The Asian monsoon over the past 640,000 years and ice age terminations. *Nature* **541**, 640–646.

Cheng, H., Zhang, H.W., Spotl, C., Baker, J., Sinha, A., Li, H.Y., Bartolome, M., *et al.*, 2020. Timing and structure of the Younger Dryas event and Its underlying climate dynamics. *Proceedings of the National Academy of Sciences* **117**, 23408–23417.

Chevalier, M.L., Replumaz, A., 2019. Deciphering old moraine age distributions in SE Tibet showing bimodal climatic signal for glaciations: Marine Isotope Stages 2 and 6. *Earth and Planetary Science Letters* **507**, 105–118.

Chevalier, M.L., Hilley, G., Tapponnier, P., Woerd, J.V.D., Zeng, J.L., Finkel, R.C., Ryerson, F.J., Li, H.B., Liu, X.H., 2011. Constraints on the late Quaternary glaciations in Tibet from cosmogenic exposure ages of moraine surfaces. *Quaternary Science Reviews* **30**, 528–554.

Chevalier, M.L., Leloup, P.H., Replumaz, A., Pan, J., Liu, D., Li, H., Gourbet, L., Métois, M., 2016. Tectonic-geomorphology of the Litang fault system, SE Tibetan Plateau, and implication for regional seismic hazard. *Tectonophysics* **682**, 278–292.

Chevalier, M.L., Leloup, P.H., Replumaz, A., Pan, J.W., 2018. Temporally constant slip rate along the Ganzi fault, NW Xianshuihe fault system, eastern Tibet. *Geological Society of America Bulletin* **130**, 396–410.

Chevalier, M.L., Replumaz, A., Wang, S.G., Pan, J.W., Bai, M.K., Li, K.Y., Li, H.B., 2022a. Limit of monsoonal precipitation in southern Tibet during the Last Glacial Maximum from relative moraine extents. *Geomorphology* **397**, 108012. https://doi.org/10.1016/j.geomorph.2021.108012.

Chevalier, M.L., Wang, S.G., Replumaz, A., Li, H.B., 2022b. Marine Oxygen Isotope Stage (MIS)-6 glacial advances on the Tibetan Plateau more extensive than during MIS-2 due to more abundant precipitation. *Acta Geologica Sinica* (*English Edition*) **96**, 1484–1494.

Dielforder, A., Hetzel, R., 2014. The deglaciation history of the Simplon region (southern Swiss Alps) constrained by ^{10}Be exposure dating of ice-molded bedrock surfaces. *Quaternary Science Reviews* **84**, 26–38.

Dong, G.C., Yi, C.L., Caffee, M., 2014. ^{10}Be dating of boulders on moraines from the last glacial period in the Nyainqentanglha Mountains, Tibet. *Science China* (*Earth Sciences*) **57**, 221–231.

Dong, G.C., Zhou W.J., Fu, Y.C., Zhang, L., Zhao, G.Q., Li, M., 2020. The last glaciation in the headwater area of the Xiaokelanhe River, Chinese Altai: evidence from ^{10}Be exposure-ages. *Quaternary Geochronology* **56**, 101054. https://doi.org/10.1016/j.quageo.2020.101054.

Dong, G.C., Zhou W.J., Xian, F., Fu, Y.C., Zhang, L., Ding, P.K., Zhao, G.Q., Li, M., 2022. Timing and climatic drivers for the MIS 6 glaciation in the central Himalaya: ^{10}Be surface exposure dating of hummocky moraine northwest of Mt. Gang Benchhen, Paiku Gangri. *Palaeogeography, Palaeoclimatology, Palaeoecology* **605**, 111230. https://doi.org/10.1016/j.palaeo.2022.111230.

Dortch, J.M., Owen, L.A., Caffee, M.W., 2013. Timing and climatic drivers for glaciation across semi-arid western Himalayan–Tibetan orogen. *Quaternary Science Reviews* **78**, 188–208.

Dortch, J.M., Tomkins, M.D., Saha, S., Murari, M.K., Schoenbohm, L.M., Curl, D., 2022. A tool for the ages: the probabilistic cosmogenic age analysis tool (P-CAAT). *Quaternary Geochronology* **7**, 101323. https://doi.org/10.1016/j.quageo.2022.101323.

Duller, G.A.T., 2006. Single grain optical dating of glacigenic deposits. *Quaternary Geochronology* **1**, 296–304.

Finkel, R.C., Owen, L.A., Barnard, P.L., Caffee, M.W., 2003. Beryllium-10 dating of Mount Everest moraines indicates a strong monsoon influence and glacial synchroneity throughout the Himalaya. *Geology* **31**, 561–564.

Fu, P., Stroeven, A.P., Harbor, J.M., Hättestrand, C., Heyman, J., Caffee, M.W., Zhou, L.P., 2013. Paleoglaciation of Shaluli Shan, southeastern Tibetan Plateau. *Quaternary Science Reviews* **64**, 121–135.

Gosse, J.C., Phillips, F.M., 2001. Terrestrial in situ cosmogenic nuclides: theory and application. *Quaternary Science Reviews* **20**, 1475–1560.

Graf, A.A., Strasky, S., Zhao, Z.Z., Akar, N., Ivy-Ochs, S., Kubik, P.W., Christl, M., Kasper, H.U., Wieler, R., Schlüchter, C., 2008. Glacier extension on the eastern Tibetan Plateau in response to MIS 2 cooling, with a contribution to ^{10}Be and ^{21}Ne methodology. In: Strasky, S., *Glacial Response to Global Climate Changes: Cosmogenic Nuclide Chronologies*

from High and Low Latitudes [submitted to *Quaternary Geochronology*]. DSc Thesis, ETH Zürich, University of Bern, Bern, Switzerland, pp. 77–110.

Gribenski, N., Jansson, K.N., Preusser, F., Harbor, J.M., Stroeven, A.P., Trauerstein, M., Blomdin, R., *et al.*, 2017. Re-evaluation of MIS 3 glaciation using cosmogenic radionuclide and single grain luminescence ages, Kanas Valley, Chinese Altai. *Journal of Quaternary Science* **33**, 55–67.

Gupta, A.K., Singh, R.K., Dutt, S., Cheng, H., Clemens, S.C., Kathayat, G., 2021. High-frequency shifts in the Indian summer monsoon following termination of the YD event. *Quaternary Science Reviews* **259**, 106888. https://doi.org/10.1016/j.quascirev.2021.106888.

Haldorsen, S., 1981. Grain-size distribution of subglacial till and its realtion [sic] to glacial scrushing and abrasion. *Boreas* **10**, 91–105.

Herzschuh, U., 2006. Palaeo-moisture evolution in monsoonal Central Asia during the last 50,000 years. *Quaternary Science Reviews* **25**, 163–178.

Heyman, J., 2014. Paleoglaciation of the Tibetan Plateau and surrounding mountains based on exposure ages and ELA depression estimates. *Quaternary Science Review* **91**, 30–41.

Heyman, J., Stroeven, A.P., Harbor, J.M., Caffee, M.W., 2011. Too young or too old: evaluating cosmogenic exposure dating based on an analysis of compiled boulder exposure ages. *Earth and Planetary Science Letters* **302**, 71–80.

Hong, Y.T., Hong, B., Lin, Q.H., Zhu, Y.X., Shibata, Y., Hirota, M., Uchida, M., *et al.*, 2003. Correlation between Indian Ocean summer monsoon and North Atlantic climate during the Holocene. *Earth and Planetary Science Letters* **211**, 371–380.

Hu, G., Yi, C.L., Zhang, J.F., Dong, G.C., Liu, J.H., Xu, X.K., Jiang, T., 2017. Extensive glacial advances during the Last Glacial Maximum near the eastern Himalayan syntaxis. *Quaternary International* **443**, 1–12.

Hughes, P.D., Gibbard, P.L., Woodward, J.C., 2005. Quaternary glacial records in mountain regions: a formal stratigraphical approach. *Episodes* **28**, 85–92.

Immerzeel, W.W., Beek, L.P.H., Bierkens, M.F.P., 2010. Climate change will affect the Asian Water Towers. *Science* **328**, 1382–1385.

Kohl, C.P., Nishiizumi, K., 1992. Chemical isolation of quartz for measurement of in-situ-produced cosmogenic nuclides. *Geochimica et Cosmochimica Acta* **56**, 3583–3587.

Kong, P., Na, C.G., Fink, D., Zhao, X.T., Xiao, W., 2009. Moraine dam related to late Quaternary glaciation in the Yulong Mountains, southwest China, and impacts on the Jinsha River. *Quaternary Science Reviews* **28**, 3224–3235.

Lal, D., 1991. Cosmic ray labeling of erosion surfaces: in situ nuclide production rates and erosion models. *Earth and Planetary Science Letters* **104**, 424–439.

Li, Y.K., 2013. Determining topographic shielding from digital elevation models for cosmogenic nuclide analysis: a GIS approach and field validation. *Journal of Mountain Science* **10**, 355–362.

Li, Y.K., Liu, G.N., Kong, P., Harbor, J., Chen, Y.X., Caffee, M., 2011. Cosmogenic nuclide constraints on glacial chronology in the source area of the Urumqi River, Tian Shan, China. *Journal of Quaternary Science* **26**, 297–304.

Li, Y.K., Liu, G.N., Chen, Y.X., Li Y.N., Harbor, J., Stroeven, A.P., Caffee, M., Zhang, M., Li C.C., Cui, Z.J., 2014. Timing and extent of Quaternary glaciations in the Tianger Range, eastern Tian Shan, China, investigated using ^{10}Be surface exposure dating. *Quaternary Science Reviews* **98**, 7–23.

Lifton, N., Sato, T., Dunai, T.J., 2014. Scaling in situ cosmogenic nuclide production rates using analytical approximations to atmospheric cosmic-ray fluxes. *Earth and Planetary Science Letters* **386**, 149–160.

Lisiecki, L.E., Raymo, M.E., 2005. A Pliocene–Pleistocene stack of 57 globally distributed benthic δ^{18}O records. *Paleoceanography* **20**, PA1003. https://doi.org/10.1029/2004PA001071.

Liu, B.B., Cui Z.J., Peng, X., Han, Y.S., Liu, G.N., 2018. Using ^{10}Be exposure dating to constrain glacial advances during the late glacial and Holocene on Mount Xuebaoding, eastern Tibetan Plateau. *Quaternary Research* **90**, 348–359.

Marcott, S.A., Bauska, T.K., Buizert, C., Steig, E.J., Rosen, J.L., Cuffey, K.M., Fudge, T.J., *et al.*, 2014. Centennial-scale changes in the global carbon cycle during the last deglaciation. *Nature* **514**, 616–619.

Murari, M.K., Owen, L.A., Dortch, J.M., Caffee, M.W., Dietsch, C., Fuchs, M., Haneberg, W.C., Sharma, M.C., Townsend-Small, A., 2014. Timing and climatic drivers for glaciation across monsoon-influenced regions of the Himalayan–Tibetan orogen. *Quaternary Science Reviews* **88**, 159–182.

Nishiizumi, K., Imamura, M., Caffee, M.W., Southon, J.R., Finkel, R.C., McAninch, J., 2007. Absolute calibration of ^{10}Be AMS standards. *Nuclear Instruments and Methods in Physics Research Section B: Beam Interactions with Materials and Atoms* **258**, 403–413.

Ou, X.J., Lai, Z.P., Zhou, S.Z., Chen, R., Zeng, L.H., 2015. Optical dating of young glacial sediments from the source area of the Urumqi River in Tianshan Mountains, northwestern China. *Quaternary International* **358**, 12–20.

Owen, L.A., 2009. Latest Pleistocene and Holocene glacier fluctuations in the Himalaya and Tibet. *Quaternary Science Reviews* **28**, 2150–2164.

Owen, L.A., Benn, D.I., 2005. Equilibrium-line altitudes of the Last Glacial Maximum for the Himalaya and Tibet: an assessment and evaluation of results. *Quaternary International* **138**, 55–78.

Owen, L.A., Dortch, J.M., 2014. Nature and timing of Quaternary glaciation in the Himalayan–Tibetan Orogen. *Quaternary Science Reviews* **88**, 14–54.

Owen L.A., Finkel R.C., Barnard, P.L., Ma H.Z., Asahi, K., Caffee, M.W., Derbyshire, E., 2005. Climatic and topographic controls on the style and timing of Late Quaternary glaciation throughout Tibet and the Himalaya defined by ^{10}Be cosmogenic radionuclide surface exposure dating. *Quaternary Science Reviews* **24**, 1391–1411.

Owen, L.A., Robinson, R., Benn, D.I., Finkel, R.C., Davis, N.K., Yi, C.L., Putkonen, J., Li, D.W., Murray, A.S., 2009. Quaternary glaciation of Mount Everest. *Quaternary Science Reviews* **28**, 1412–1433.

Pellitero, R., Rea, B.R., Spagnolo, M., Bakke, J., Hughes, P., Ivy-Ochs, S., Lukas, S., Ribolini, A., 2015. A GIS tool for automatic calculation of glacier equilibrium-line altitudes. *Computers & Geosciences* **82**, 55–62.

Pellitero, R., Rea, B.R., Spagnolo, M., Bakke, J., Ivy-Ochs, S., Frew, C.R., Hughes, P., Ribolini, A., Lukas, S., Renssen, H., 2016. GlaRe, a GIS tool to reconstruct the 3D surface of palaeoglaciers. *Computers & Geosciences* **94**, 77–85.

Porter, S.C., 1975. Glaciation limit in New Zealand's Southern Alps. *Arctic and Alpine Research* **7**, 33–37.

Preffer, W.T., Arendt, A., Bliss, A., Bolch, T., Cogley, J.G., Gardner, A.S., Hagen, J.-O., *et al.*, 2014. The Randolph Glacier inventory; a globally complete inventory of glaciers. *Journal of Glaciology* **60**, 537–552.

Rea, B.R., 2009. Defining modern day area-altitude balance ratios (AABRs) and their use in glacier–climate reconstructions. *Quaternary Science Reviews* **28**, 237–248.

Richards, B.W.M., 2000. Luminescence dating of Quaternary sediments in the Himalaya and High Asia: a practical guide to its use and limitations for constraining the timing of glaciation. *Quaternary International* **65–66**, 49–61.

Saha, S., Owen, L.A., Orr, E.N., Caffee, M.W., 2018. Timing and nature of Holocene glacier advances at the northwestern end of the Himalayan–Tibetan orogen. *Quaternary Science Reviews* **187**, 177–202.

Saha, S., Owen, L.A., Orr, E.N., Caffee, M.W., 2019. High-frequency Holocene glacier fluctuations in the Himalayan–Tibetan orogen. *Quaternary Science Reviews* **220**, 372–400.

Schäfer, J.M., Tschudi, S., Zhao, Z.Z., Wu, X.H., Ivy-Ochs, S., Wieler, R., Heinrich, B., Kubik, P.W., Schlüchter, C., 2002. The limited influence of glaciations in Tibet on global climate over the past 170,000 yr. *Earth and Planetary Science Letters* **194**, 287–297.

Schneider, R., Schmitt, J., Koehler, P., Joos, F., Fischer, H., 2013. A reconstruction of atmospheric carbon dioxide and its stable carbon isotopic composition from the penultimate glacial maximum to the glacial inception. *Climate of the Past* **9**, 2507–2523.

Seong, Y.B., Owen, L.A., Yi, C.L., Finkel, R.C., 2009. Quaternary glaciation of Muztag Ata and Kongur Shan: evidence for glacier response to rapid climate changes throughout the Late Glacial and Holocene in westernmost Tibet. *Geological Society of America Bulletin* **121**, 348–365.

Shi, Y.F., 2002. Characteristics of late Quaternary monsoonal glaciation on the Tibetan Plateau and in East Asia. *Quaternary International* **97–98**, 79–91.

Sigman, D.M., Hain, M.P., Haug, G.H., 2010. The polar ocean and glacial cycles in atmospheric CO_2 concentration. *Nature* **466**, 47–55.

https://doi.org/10.1017/qua.2023.45 Published online by Cambridge University Press

Solomina, O.N., Bradley, R.S., Hodgson, D.A., Ivy-Ochs, S., Jomelli, V., Mackintosh, A.N., Nesje, A., *et al.*, 2015. Holocene glacier fluctuations. *Quaternary Science Reviews* **111**, 9–34.

Stone, J.O., 2000. Air pressure and cosmogenic isotope production. *Journal of Geophysical Research* **105**, 23753–23759.

Strasky, S., Graf, A.A., Zhao, Z., Kubik, P.W., Baur, H., Schlüchter, C., Wieler, R., 2009. Late Glacial ice advances in southeast Tibet. *Journal of Asian Earth Sciences* **34**, 458–465.

Su, Z., Pu, J.C., 1996. Development conditions, number and morphological characteristics of glaciers in the Hengduan Mountains region. In: Li, J.J., Su, Z. (Eds.) *Glaciers in the Hengduan Mountains*. Science Press, Beijing, pp. 1–21.

Tang, L.Y., Shen, C.M., Liao, G.B., Overpeck, J.T., Yu, Y.S., 2000. Climatic and hydrological changes in the southeastern Qinghai–Tibetan Plateau during the past 18000 years. *Acta Micropalaeontologica Sinica* **17**, 113–124.

Tang, L.Y., Shen, C.M., Liu, K.B., Yu, S.R., Liu, C.H., 2004. Climatic changes since the Last Glacial Maximum in the southeastern Tibetan Plateau: pollen evidence. *Science in China* **34**, 434–442.

Thompson, L.G., Davis, M.E., Mosley-Thompson, E., Henderson, K., Lin, P.-N., Mashiotta, T., 2005. Tropical ice core records: evidence for asynchronous glaciation on Milankovitch timescales. *Journal of Quaternary Science* **20**, 723–733.

Wang J., 2010. Glacial advance in the QingHai–Tibet Plateau and peripheral mountains during the mid-MIS-3. *Quaternary Sciences* **30**, 1055–1065. [in Chinese, with English abstract]

Wang, J., Raisbeck, G., Xu, X., Yiou, F., Bai, S., 2006. In situ cosmogenic ^{10}Be dating of the Quaternary glaciations in the southern Shaluli Mountain on the southeastern Tibetan Plateau. *Science in China Series D: Earth Sciences* **49**, 1291–1298.

Wang, J., Cui, H., Harbor, J.M., Zheng, L.M., Yao, P., 2015. Mid-MIS3 climate inferred from reconstructing the Dalijia Shan ice cap, northeastern Tibetan Plateau. *Journal of Quaternary Science* **30**, 558–568.

Wang, J., Wang, W.C., Cao, B., Cui, H., Chen, X.J., Qiu, J.K., Lei, M.H., Liao, J.S., 2023. Millennial-scale glacier fluctuations on the southeastern Tibetan Plateau during MIS 2. *Earth and Planetary Science Letters* **601**, 117903. https://doi.org/10.1016/j.epsl.2022.117903.

Wang, Y.J., Cheng, H., Edwards, R.L., He, Y.Q., Kong, X.G., An, Z.S., Wu, J.Y., Kelly, J., Dykoski, C.A., Li, X.D., 2005. The Holocene Asian Monsoon: links to solar changes and North Atlantic climate. *Science* **308**, 854–857.

Wang, Y.J., Cheng, H., Edwards, R.L., Kong, X.G., Shao, X.H., Chen, S.T., Wu, J.Y., Jiang, XJ., Wang, X.F., An, Z.S., 2008. Millennial- and orbital-scale changes in the East Asian monsoon over the past 224,000 years. *Nature* **451**, 1090–1093.

Wanner, H., Solomina, O., Grosjean, M., Ritz, S.P., Jetel, M., 2011. Structure and origin of Holocene cold events. *Quaternary Science Reviews* **30**, 3109–3123.

Xu, L.B., Ou, X.J., Lai, Z.P., Zhou, S.Z., Wang, J., Fu, Y.C., 2010. Timing and style of Late Pleistocene glaciation in the Queer Shan, northern Hengduan Mountains in the eastern Tibetan Plateau. *Journal of Quaternary Science* **25**, 957–966.

Xu, X.K., Glasser, N.F., 2015. Glacier sensitivity to equilibrium line altitude and reconstruction for the Last Glacial cycle: glacier modeling in the Payuwang Valley, western Nyaiqentanggulha Shan, Tibetan Plateau. *Palaeogeography, Palaeoclimatology, Palaeoecology* **440**, 614–620.

Yao, T.D., Thompson, L.G., Mosbrugger, V., Zhang, F., Ma, Y.M., Luo, T.X., Xu, B.Q., *et al.*, 2012. Third pole environment (TPE). *Environmental Development* **3**, 52–64.

Yi, C.L., Jiao, K.Q., Liu, K.X., He, Q.C., Ye, Y.G., 2002. ESR dating of the sediments of the last glaciation at the source of the Urumqi River, Tian Shan Mountains, China. *Quaternary International* **97/98**, 141–146.

Yi, C.L., Bi, W.L., Li, J.P., 2016. ESR dating of glacial moraine deposits: some insights about the resetting of the germanium (Ge) signal measured in quartz. *Quaternary Geochronology* **35**, 69–76.

Zeng L.H., Ou X.J., Chen, R., Lai, Z.P., 2019. OSL dating on glacial sediments of the Last Glacial in headwater of Urumqi River, Tianshan Mountains. *Journal of Glaciology and Geocryology* **41**, 761–769. [in Chinese, with English abstract]

Zhang, W., Chai, L., 2016. The preliminary study of the Quaternary glacier in middle part of the Tenasserim Chain with ESR dating method. *Journal of Glaciology and Geocryology* **38**, 1281–1291. [in Chinese, with English abstract]

Zhang, W., Liu, L., Chen, Y.X., Liu, B.B., Harbor, J.M., Cui, Z.J., Liu, R., Liu, X., Zhao, X., 2016. Late glacial ^{10}Be ages for glacial landforms in the upper region of the Taibai glaciation in the Qinling Mountain range, China. *Journal of Asian Earth Sciences* **115**, 383–392.

Zhang, W., Chai, L., Evans, I.S., Li, Y.P., Qiao, J.R., Tang, Q.Y., Sun, B., 2019. Geomorphic features of Quaternary glaciation in the Taniantaweng Mountain, on the southeastern Qinghai–Tibet Plateau. *Journal of Mountain Science* **16**, 256–274.

Zhang, Z.G., Wang, J., Xu, X.B., Bai, S.B., Chang, Z.Y., 2015. Cosmogenic ^{10}Be and ^{26}Al chronology of the last glaciation of the palaeo-Daocheng Ice Cap, southeastern Qinghai–Tibetan Plateau. *Acta Geologica Sinica* (*English Edition*) **89**, 575–584.

Zhao, J.D., Zhou, S.Z., Liu, S.Y., He, Y.Q., Xu, L.B., Wang, J., 2007. A preliminary study of the glacier advance in MIS3b in the western regions of China. *Journal of Glaciology and Geocryology* **29**, 233–241. [in Chinese, with English Abstract]

Zhao, J.D., Song, Y.G., King, J.W., Liu, S.Y., Wang, J., Wu, M., 2010. Glacial geomorphology and glacial history of the Muzart River Valley, Tianshan Range, China. *Quaternary Science Reviews* **29**, 1453–1463.

Zhou, S.Z., Li, J.J., Zhang, S.Q., 2002. Quaternary glaciation of the Bailang River Valley, Qilian Shan. *Quaternary International* **97–98**, 103–110.

Zhou, S.Z., Xu, L.B., Colgan, P.M., Mickelson, D.M., Wang, X.L., Wang, J., Zhong, W., 2007. Cosmogenic ^{10}Be dating of Guxiang and Baiyu glaciations. *Chinese Science Bulletin* **52**, 1387–1393.

https://doi.org/10.1017/qua.2023.45 Published online by Cambridge University Press